Faculty and Researchers | Faculty and Researchers' Publications

2010

Wintertime mixed layer measurements at Maud Rise, Weddell Sea

Sirevaag, Anders; McPhee, Miles G.; Morison, James H.; Shaw, William J.; Stanton, Timothy P.

American Geophysical Union

Wintertime mixed layer measurements at Maud Rise, Weddell Sea

Anders Sirevaag,[1,2] Miles G. McPhee,[3] James H. Morison,[4] William J. Shaw,[5]
and Timothy P. Stanton[5]

[1] Sea ice plays a crucial role in the exchange of heat between the ocean and the atmosphere, and areas of intense air-sea-ice interaction are important sites for water mass modification. The Weddell Sea is one of these sites where a relatively thin first-year ice cover is constantly being changed by mixing of heat from below and stress exerted from the rapidly changing and intense winds. This study presents mixed layer turbulence measurements obtained during two wintertime drift stations in August 2005 in the eastern Weddell Sea, close to the Maud Rise seamount. Turbulence in the boundary layer is found to be controlled by the drifting ice. Directly measured heat fluxes compare well with previous studies and are well estimated from the mixed layer temperatures and mixing. Heat fluxes are also found to roughly balance the conductive heat flux in the ice; hence, little freezing/melting was observed. The under-ice topography is estimated to be hydraulically very smooth; comparison with a steady 1-D model shows that these estimates are made too close to the ice-ocean interface to be representative for the entire ice floe. The main source and sink of turbulent kinetic energy are shear production and dissipation. Observations indicate that the dynamics of the under-ice boundary layer are influenced by a horizontal variability in mixed layer density and an increasing amount of open leads in the area.

1. Introduction

[2] The Weddell Sea is considered one of the prominent sites for production of ocean deep water, produced both on the large shelf areas and by open ocean convection. The potential for the latter is caused by an often thin and weak pycnocline that separates the mixed layer from the warmer water below, a pycnocline that is easily eroded as wind-induced mixing increases or convection caused by salt release from growing ice occurs [*Gordon*, 1991]. Removing this pycnocline and bringing warm water toward the surface melts the ice and initiates a massive exchange of heat from the ocean to the atmosphere. The Weddell Polynya that occurred in the mid-1970s serves as a prime example of this state of extreme air-sea-ice interaction [*Carsey*, 1980; *Gordon*, 1978; *Zwally and Gloersen*, 1977]. This polynya persisted over several winters and had its origin around Maud Rise, a topographic feature in the eastern Weddell Sea centered at 65°S, 3°E. In this area, relatively warm Weddell Deep Water flows onto the topographic feature and introduces heat and salt that can be mixed upward and can affect

ice formation, stability, and fluxes of heat, salt, and momentum in the surface layer [*Gordon*, 1991]. Hydrographically, the water column around Maud Rise has two distinct features: The northern and western flanks of the rise are surrounded by a halo in which the water column has a relatively high temperature maximum ($T_{max} > 1°C$) and salinity maximum ($S_{max} > 34.7$) and a relatively shallow mixed layer, often designated Halo water [*de Steur et al.*, 2007; *Muench et al.*, 2001]. The water column on top of the rise itself is a Taylor column with lower T_{max}, S_{max}, and static stability and a deeper pycnocline, the so-called Taylor Cap water [*Gordon and Huber*, 1990; *Muench et al.*, 2001]. The low-stability water column implies that mixing processes at the pycnocline and in the mixed layer are of great importance.

[3] In recent decades, instrumentation has improved facilitating direct in situ measurements of turbulence and mixing. Drifting sea ice offers a convenient stable platform for such measurements. Several drifting experiments in the Weddell Sea have been conducted [*McPhee and Martinson*, 1994; *McPhee et al.*, 1996; *McPhee*, 2008a] focusing on small-scale dynamics and scalar fluxes in the mixed layer. One of these experiments, the Antarctic Zone Flux Experiment (ANZFLUX [*McPhee et al.*, 1996]), was performed in the Maud Rise area in the austral winter of 1994, offering detailed measurements in this potentially unstable water column covered only by a relatively thin layer of first-year ice. *McPhee et al.* [1996] found that heat fluxes under these conditions could be determined from mixed layer temper-

[1]Geophysical Institute, University of Bergen, Bergen, Norway.
[2]Also at Bjerknes Centre for Climate Research, Bergen, Norway.
[3]McPhee Research Company, Naches, Washington, USA.
[4]Polar Science Center, Applied Physics Laboratory, University of Washington, Seattle, Washington, USA.
[5]Naval Postgraduate School, Monterey, California, USA.

ature elevation above freezing, friction velocity, and a turbulent exchange coefficient that was more or less similar as for heat fluxes under thick Arctic pack ice [*McPhee*, 1992; *McPhee et al.*, 1999]. Heat fluxes were on average about 27 W m^{-2}; however, they showed a large temporal variation with varying atmospheric and hydrographic conditions. In addition, it was found that the under-ice roughness length was about two orders of magnitude smaller than for Arctic pack ice conditions, hence reducing the stress exerted on the water column by the drifting ice. The ice cover's response to wind forcing was more rapid with an ice drift-wind ratio up to twice as large as for Arctic pack ice [*McPhee et al.*, 1996], as expected for ice with relatively smooth under-ice topography.

[4] On the basis of the potential for deep convection caused by increased salinity in the mixed layer and by nonlinear instabilities in the pycnocline [*Akitomo*, 1999a, 1999b; *McPhee*, 2000], a new field campaign was launched in the austral winter of 2005. The Maud Rise Nonlinear Equation of State Study (MaudNESS) experiment was designed to make detailed observations in the upper ocean as the water column preconditioned for possible deep convection. It consisted of several phases: The first phase was a conductivity-temperature-depth (CTD) survey mapping the hydrography over Maud Rise to find the areas where onset of deep convection was most likely [*de Steur et al.*, 2007]. The second phase consisted of two ice-based drift stations where measurements of the entire upper ocean were made. In the third phase, potentially unstable water masses found during the first phase were tracked, and small-scale measurements were made using ship-based instrument systems in drifts with typical durations of 1 day. A central part of the design strategy for MaudNESS was that phase 3 would concentrate on rapid deployments in marginal conditions for which it might be both unsafe and untimely to put instrumentations and observers on the ice. However, deploying all the instrumentation from the ship in phase 3 dictated that we would be unable to make measurements in the upper part of the boundary layer. We anticipated that phase 2, with direct measurements of near-surface fluxes away from the disturbing influence of the ship, would provide "ground truth" for estimating similar fluxes during phase 3.

[5] This paper explores phase 2 measurements by considering data from two ice-based drift stations, designated P2D1 and P2D2. It is organized as follows: In section 2, the instrumentation will be described along with descriptions of the two drifts. In section 3, the general hydrographic conditions and turbulent fluxes will be presented, and small-scale dynamics and turbulence parameters will be analyzed, discussed, and compared with a 1-D steady state turbulence model in section 4. Summary and concluding remarks are given in section 5.

2. Experimental Setup

2.1. Instrumentation

[6] Central in the MaudNESS upper boundary layer measurement program was the use of turbulence instrument clusters (TICs [see also *McPhee*, 2008b]), designed to measure turbulence and turbulent fluxes below the ice. Each

TIC consists of a Sontek/YSI acoustic Doppler velocimeter (ADV) to measure 3-D velocities, a fast-response SBE-3 temperature sensor, and a dual-needle SBE-7 microconductivity (subsequently referred to as μC) sensor, all manufactured by Sea-Bird Electronics. All these sensors are mounted on a mast to measure in the same vertical level. In addition, an SBE-4 conductivity cell (subsequently referred to as stdC), also from Sea-Bird Electronics, is mounted about 20 cm above the others to provide high-quality measurements of the absolute salinity but to not disturb the flow across the instrument. During MaudNESS, TICs were deployed in two configurations. The so-called shallow mast contained one TIC and was suspended using rigid poles fixed to the ice, and the mast had to be rotated manually to direct sensors into the mean flow. The midlevel turbulence mast supported two TICs mounted with a vertical spacing of 4 m; only the upper TIC had a μC sensor and was suspended using a wire. This allowed it to be positioned deeper in the boundary layer and to rotate freely to always be directed toward the mean current.

[7] The open needle construction of the μC sensor makes it susceptible to biofouling, which can introduce spurious jumps in measured conductivity. It is also subject to a considerable drift in absolute conductivity over a relatively short time, which can be troublesome when calculating salinity. To solve these problems, periods with significant jumps in conductivity were removed, and absolute conductivity measured by the stdC sensor was used to adjust the mean conductivity from the μC sensor to the ambient conductivity.

[8] The ship was equipped with a 150 KHz acoustic Doppler current profiler (ADCP). ADCP data were post-processed by the University of Hawaii and were made available as 5 min averages of horizontal velocity in depth bins of 8 m, ranging from 35 m below the surface and with good quality at least throughout the mixed layer. ADCP measurements were continuous; however, they can be distorted by ice under the ship, which happened in shorter periods during P2D2.

[9] A second profiling instrument, a Sontek acoustic Doppler profiler (ADP), was deployed near the shallow mast during P2D2. When deployed from the ice, this ADP can provide measurements relatively close to the surface, an advantage compared with the ship-mounted ADCP. The downward looking ADP was deployed less than 1 m below the ice and measured velocity profiles every 30 s, averaged in 2 m depth cells from 3 m below the ice and with good quality down to 29 m below the ice. For this work, velocities were adjusted for the local magnetic declination, which in the Maud Rise region was 21°W, and were averaged over 1 h.

[10] In addition to the temperature and salinity measurements provided by the TICs, an automated cycling CTD profiler was used to gain information about the mixed layer hydrography. The CTD profiler, a SeaBird SBE19plus, was deployed using an automated winch and provided profiles of temperature and salinity every 10 min. Individual CTD profiles were averaged in 2 m depth bins.

[11] This study also utilizes position data from the ship's GPS system in addition to air temperature and wind measurements made 17 m and 32 m above sea level, all
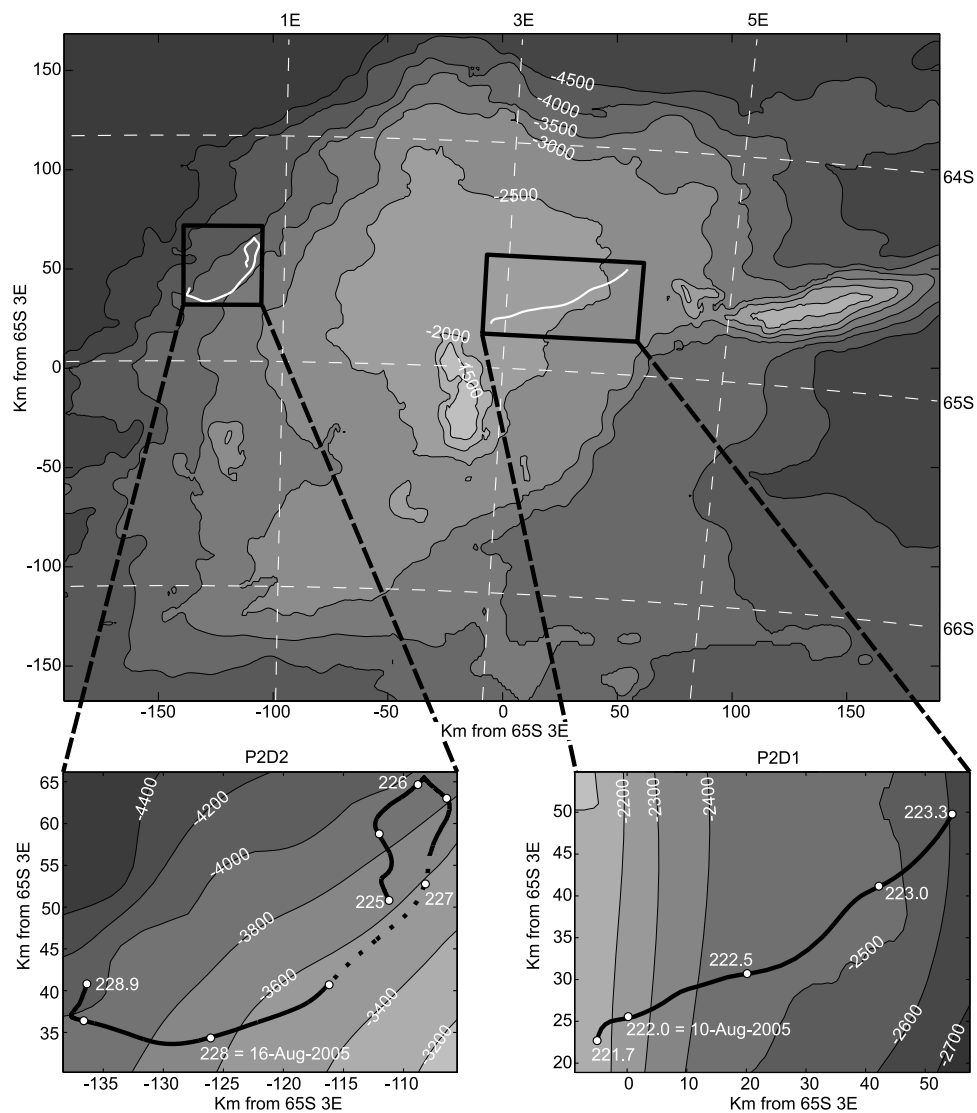
Figure 1. (top) Bathymetry of the Maud Rise from the General Bathymetric Chart of the Oceans (GEBCO) bathymetry (reproduced from the *GEBCO Digital Atlas* published by the British Oceanographic Data Centre on behalf of the Intergovernmental Oceanographic Commission and International Hydrographic Organization in 2003) in a polar stereographic grid centered at 65°S, 3°E. (bottom) Magnified drift trajectories with time stamps. The dashed line in the P2D2 trajectory indicates when the instruments were relocated.

available via the ship's data acquisition system. Wind speeds from 17 m height were adjusted to 10 m values following *Smith* [1988].

2.2. Drift Descriptions

[12] The first drift, P2D1, took place over the eastern half of the Maud Rise seamount, from 9 August 1600 UTC to 11 August 0800 UTC. P2D2 was over the western flank of the seamount, from 12 August 1500 UTC to 16 August 2200 UTC. In the following, the time convention "year day" will be used, where day 1.5 corresponds to 1 January 1200 UTC. Figure 1 shows the trajectories of both drifts plotted on top of the bathymetry of Maud Rise.

[13] Ice drift velocities were obtained from the ship's GPS data. The 1 s position data were transformed into local x and y coordinates in a polar stereographic grid, rotated with the x

axis along 90°E and the y axis along 0°E and centered with the origin at 65°S, 3°E, corresponding approximately to the center of Maud Rise. For every 20 min, x and y data are transformed to a complex vector and are fitted to a second-order complex polynomial in time within this interval. The velocity is taken as the derivative of this at any time.

[14] P2D1 was established at initial position 64.81°S, 2.87°E under windy conditions and on relatively small ice floe consisting of flat first-year ice. A survey performed on day 222 determined the average ice thickness to be 39 cm with an average snow layer of 7 cm. These thicknesses are averaged over a transect of about 300 m, counting 23 individual measurement points (D. Notz and D. Goldberg, personal communication, 2005). The floe drifted northeast 67.56 km over a period of 38 h, equivalent to a mean drift velocity of 49.4 cm s^{-1}; maximum and minimum drift

velocities were 70.5 cm s^{-1} and 22.2 cm s^{-1}, respectively. Weather conditions were influenced by a low-pressure system positioned south of Maud Rise for most of the drift period, which resulted in relatively low temperatures and strong winds. Average, maximum, and minimum air temperatures were −19.6°C, −13.7°C, and −24.3°C, respectively, while the wind speed had an average of 13.3 m s^{-1} and maximum and minimum values of 17.3 m s^{-1} and 8.8 m s^{-1}, respectively. Average wind direction was 259°. The midlevel turbulence mast was deployed from time 221.9, leveled with the upper and lower TICs 2.8 m and 6.8 m below the ice-ocean interface, respectively. Unfortunately, unstable ice conditions forced a rapid recovery of all instrumentation on the ice at time 222.75. The cycling CTD profiler, which was deployed from the ship, started the measurements at time 222.6 and kept measuring until the end of the drift, i.e., day 223.3.

[15] After the end of the unstable P2D1, a vast and initially more solid floe was found for the second drift, P2D2. This drift started out on the evening of day 224 at initial position 64.58°S, 0.67°E, and the floe consisted of relatively flat ice with some small ridges and some rafted ice observed at the surface. Measurements along a 300 m long transect revealed ice thicknesses between 20 cm and 80 cm with an average ice thickness of 40 cm, and no significant melting or growth of ice was observed during the drift. The ice was covered with a layer of snow, which on average was 14 cm thick (D. Notz and D. Goldberg, personal communication, 2005). Instruments were deployed throughout the evening of day 224, and most of the upper boundary layer instruments were operating from day 225.1. The shallow turbulence mast was deployed with the TIC at 2.8 m below the ice about 300 m from the ship. The midlevel turbulence mast was deployed closer to the ship with the TIC at about 30 m depth. The ADP was deployed at the same location as the shallow mast. At time 226.82, the floe broke up and forced a recovery of the instruments farthest from the ship. Redeployment of the shallow mast and the ADP were done close to the midlevel turbulence mast, about 50 m from the ship. Most instruments operated again from 227.5 and until the end of the drift.

[16] During P2D2 (Figure 1), the ice initially drifted northward, made a sharp turn at time 226.3, then drifted southeast, turned clockwise and made another sharp turn on day 228.6, and ended up drifting northward again on the evening of day 228. The total drifted distance was 71.91 km during the 92 h of the drift, equivalent to a mean drift speed of 21.7 cm s^{-1}. Maximum and minimum ice drift speeds were 38.1 cm s^{-1} and 1.0 cm s^{-1}, respectively.

[17] The longer-lasting P2D2 offered calmer, but more varied, wind conditions. Average, maximum, and minimum wind speeds were 7.8 m s^{-1}, 11.2 m s^{-1}, and 3.2 m s^{-1}, respectively. Initial wind direction was southerly on day 225, during the drift the wind made a complete 360° clockwise rotation in direction, turning back to southerly again during day 228. The mean air temperature over the period of the drift was −18.0°C; maximum and minimum temperatures were −14.7°C and −21.9°C, respectively. Weather conditions during the drift resulted from a high-pressure system passing the ship with maximum pressure at time 226.2 and then the passing of a low-pressure system with stronger winds and minimum air pressure at time

227.7. Temperature minimum/maximum also occurred at the times of maximum/minimum air pressure.

3. Measurements
### 3.1. Mixed Layer Hydrography

[18] Figures 2 and 3 show the mixed layer depth, average mixed layer temperatures, and average mixed layer salinities for both drifts, all extracted from the cycling CTD data. Following de Steur et al. [2007], the mixed layer depth is determined as the depth where the salinity exceeds the upper layer mean salinity (50–60 m for P2D1 and 20–30 m for P2D2) by 0.02 on the practical salinity scale, hereafter abbreviated psu.

[19] During P2D1, the mean mixed layer temperature, salinity, and depth were −1.81°C, 34.46 psu, and 123 m, respectively. During the period of CTD measurements, mixed layer depth increased from initially 105 m to 150 m toward the end of the drift. In the same period, the mixed layer got slightly colder and fresher, indicating that changes in mixed layer properties were due to horizontal gradients as we drifted eastward and not due to vertical mixing. Because of a malfunctioning conductivity sensor at the TIC at 2.8 m, the salinity obtained at 6.8 m was used for P2D1. In Figure 2, TIC temperatures at 2.8 m and TIC salinities at 6.8 m are plotted, and although the overlapping period of TIC and CTD measurements was quite short, it shows that the surface layer was slightly colder and fresher than the mean mixed layer. Water masses encountered during P2D1 over the northeastern side of Maud Rise are typical Taylor Cap water with a cold mixed layer over a relatively deep pycnocline.

[20] P2D2 mixed layer depth varied from 80 m to 20 m with an average depth of 37 m, and the mixed layer was in general warmer during P2D2 with an average temperature of −1.66°C. However, instantaneous temperatures as high as −1.2°C were encountered during the drift, and an increase in temperature was followed by a decrease in salinity; average salinity was 34.48 for the whole drift. TIC temperature and salinity at 2.8 m below the ice (Figure 3) followed the mixed layer conditions in general but showed a surface layer slightly colder and fresher than the bulk mixed layer around day 226. Though not so much as P2D1, the P2D2 mixed layer was slightly more stratified in the Halo water, where the upper mixed layer was colder and fresher than the rest of the mixed layer. P2D2 took place on the flank of the Maud Rise, which is often considered the transition region between Halo water and Taylor Cap water. In Figure 3, periods where the water column met the Halo water criteria, i.e., $T_{max} > 1$°C and $S_{max} > 34.7$ [de Steur et al., 2007], are indicated with a thick horizontal line and show that we drifted from Halo water into Taylor Cap water and then slowly into Halo water again. Figure 3 shows that observed mixed layer depths do not follow definitions of Halo and Taylor Cap waters perfectly, which may indicate influence of advective effects and horizontal exchange of water masses in this area.

3.2. Mixed Layer Currents

[21] During P2D1, current measurements were provided by the ship-mounted ADCP, which covered the mixed layer below 35 m, and the TIC at 2.8 m below the ice-ocean interface. Absolute TIC velocities are found by adding the
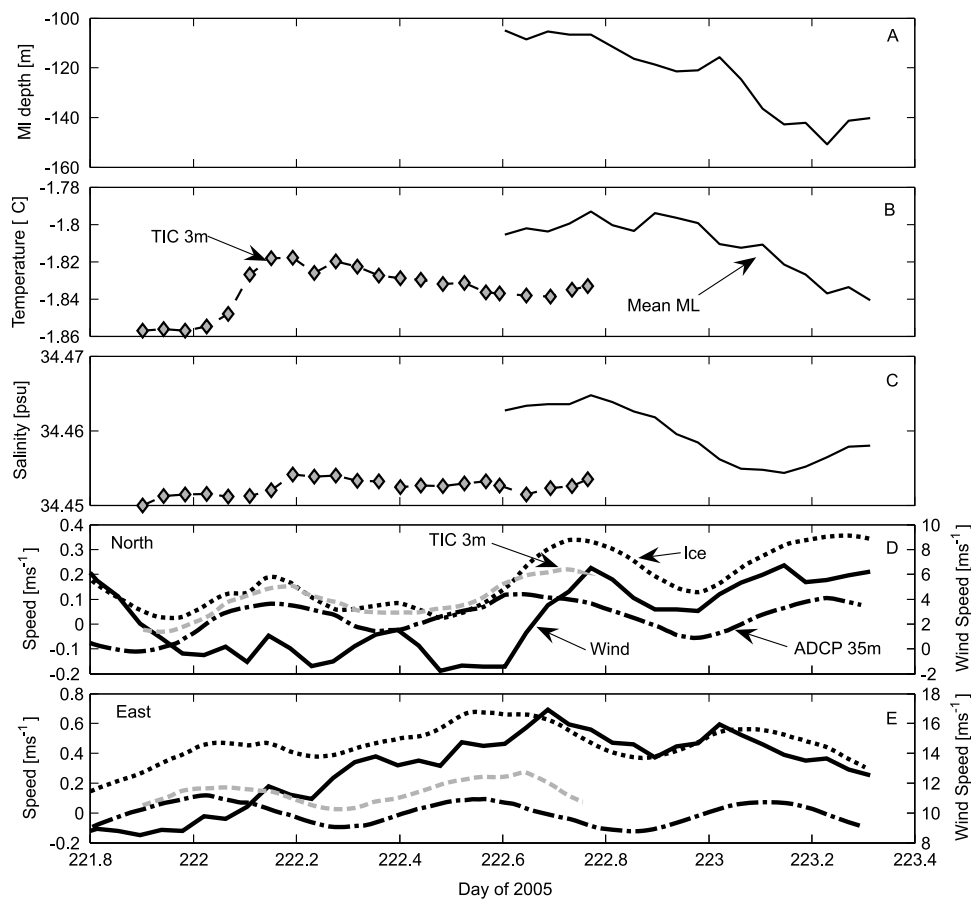
Figure 2. Mixed layer depth, mixed layer temperature, and mixed layer salinity for the P2D1 drift are shown in Figures 2a, 2b, and 2c, respectively. TIC values (diamonds) are hourly average values from 2.8 m below the ice for temperature and 6.8 m below the ice for salinity. The "mean ML" values are hourly values from the yoyo CTD and are the average of all measurements within the mixed layer. Hourly averages of northward and eastward components of wind, ice drift, and absolute current at 2.8 m below the ice and absolute currents at 35 m below the ice are shown in Figures 2d and 2e, respectively.

ice velocity. In Figure 2, hourly averages of the northerly and easterly components of currents at 2.8 m and 35 m are shown together with the components of ice drift and wind. Figure 2 shows that the upper mixed layer oscillated in phase with the ice with a period close to the inertial or semidiurnal tidal period of 13.4 h. At both 2.8 m and 35 m, absolute current velocities are well correlated with the ice velocity (correlation coefficients above 0.7). Average current speed was 12 cm s^{-1} at 35 m and 18 cm s^{-1} at 2.8 m. Since the average drift speed was 49 cm s^{-1}, most of the velocity shear was in the upper meters of the mixed layer. There was also an angular shear in the mixed layer; currents at 2.8 m were on average directed 18.5° to the left of the ice. Below the pycnocline, average ADCP velocity at 147 m (not shown here) was 3 cm s^{-1} and showed variations at the M_2 frequency, which corresponds well with the modeled estimates of the barotropic tide in the Maud Rise region [*Robertson et al.*, 1998].

[22] For P2D2, current measurements were made by the ADP that covered the range 3−29 m below the ice, in addition to the TIC at 2.8 m. For both instruments, absolute currents were found by adding the ice velocity.

[23] P2D2 had more complex wind and current conditions, but again, inertial (or semidiurnal tidal) oscillations were a

prominent feature of mixed layer velocities (Figure 3). At 29 m, average velocity was 6 cm s^{-1}, while average velocity at 2.8 m was 7 cm s^{-1}, which leaves most of the velocity shear in the upper meters of the mixed layer. As for P2D1, a significant angular shear was found in this layer; currents at 2.8 m were on average directed 24.2° to the left of the ice drift direction. ADP velocities showed a distinct turning of velocity direction in the upper 30 m, with an average turning of 12.3° from 3 m to 29 m. (see also section 4.4 and Figure 9). As for the first drift, current velocity at 2.8 m is well correlated with the ice drift velocity with a correlation coefficient of 0.74. ADP velocities at 29 m are uncorrelated with ice velocities, indicating that only the upper part of the mixed layer was oscillating in phase with the ice. A possible reason for this is the relative rapid change in water mass properties that set up horizontal density gradients resulting in baroclinic flows. Such flows were found to be present in the area of P2D2 by *de Steur et al.* [2007].

3.3. Turbulence

[24] Turbulent fluxes are calculated from the TIC at 2.8 m below the ice-ocean interface. The exception is P2D1 where salt fluxes are calculated from the TIC at 6.8 m.
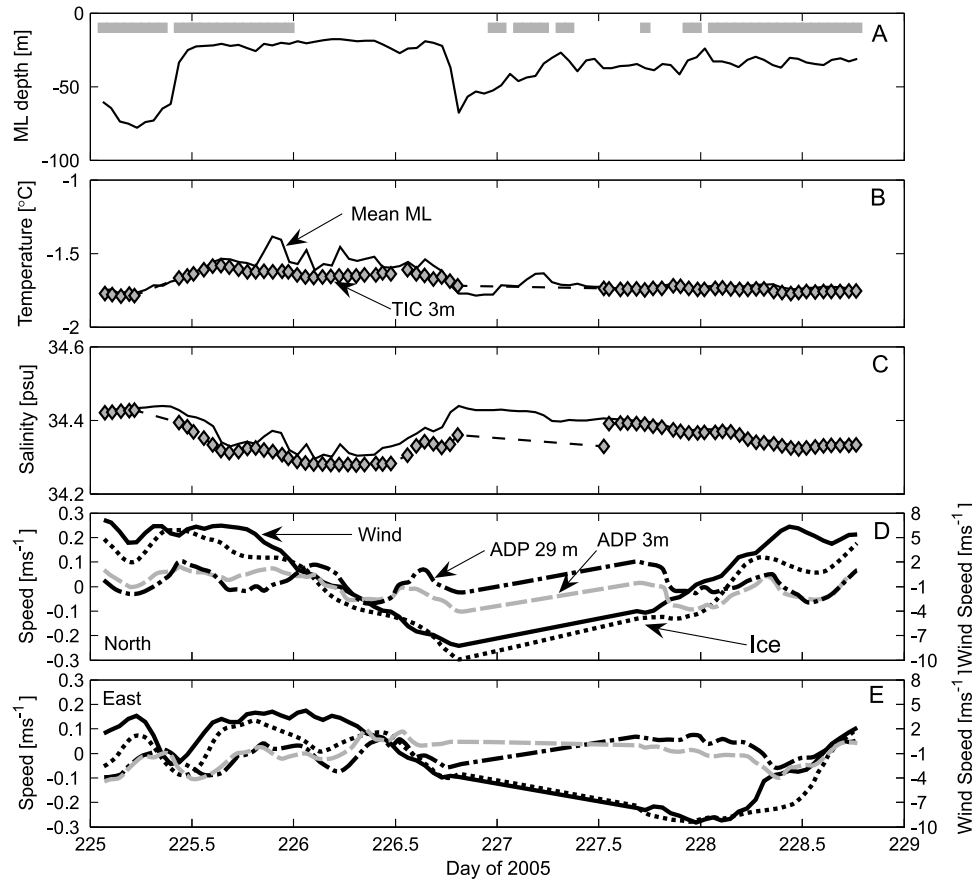
Figure 3. Mixed layer depth, mixed layer temperature, and mixed layer salinity for the P2D2 drift are shown in Figures 3a, 3b, and 3c, respectively. TIC values (diamonds) are hourly average values from 2.8 m below the ice for temperature and salinity. The red markers in the upper part indicate when the water column has Halo water properties ($T_{max} > 1°C$, $S_{max} > 34.7$). The "mean ML" values are hourly values from the yoyo CTD and are the average of all measurements within the mixed layer. Hourly averages of northward and eastward components of wind, ice drift, and absolute current at 2.8 m below the ice and absolute currents at 29 m below the ice are shown in Figures 3d and 3e, respectively.

[25] Under sea ice, turbulent-energy-containing eddies often persist for up to several minutes. To capture the covariance in these eddies but to avoid including energy contributed by processes with variability on a longer time scale, averaging intervals of 15 min were chosen. Within each of these 15 min periods, the velocity vector is rotated into a streamline coordinate system aligned with the x axis along the mean current, so that $|u| = U$, where U is the mean velocity, and $|v| = |w| = 0$; u, v, and w are the velocity components in the x, y, and z direction, respectively. Deviatory quantities of temperature, salinity, and u are obtained by linear detrending within each 15 min period, and friction velocity and fluxes of heat and salt are calculated as

$$u_* = \left(\langle u'w' \rangle^2 + \langle v'w' \rangle^2 \right)^{1/4}, \quad (1)$$

$$F_H = \rho c_p \langle w'T' \rangle, \quad (2)$$

$$F_S = \langle w'S' \rangle. \quad (3)$$

In equations (1)–(3), u_* is the kinematic friction velocity, $u_* = |\tau/\rho|^{1/2}$, and F_H and F_S are heat and salt fluxes, respectively. Furthermore, ρ is the mixed layer density and c_p is the specific heat of seawater; primes indicate deviatory quantities and brackets indicate 15 min averaging. To average out some of the variability between every realization, flux estimates are averaged in 3 h bins. For much of P2D2, the midlevel mast was deployed below the well-mixed layer, but a 24 h time span of data from 30.6 m depth (above the pycnocline) is included in this study.

[26] For P2D1, u_*, F_H, and F_S are shown in Figure 4, and average values are summarized in Table 1. Average u_* was 0.98 cm s^{-1}; however, it was increasing steadily during the whole drift, following the increase in wind and drift velocity. Considering the large drift velocities, u_* was relatively small, which indicates an ice floe with relatively smooth underside compared with multiyear pack ice in the Arctic [McPhee, 2002] and in the western Weddell Sea [McPhee, 2008a]. However, the observations are in line with other observations from the eastern Weddell Sea that have reported similar values of friction velocity under similar conditions [McPhee et al., 1999]. Turbulent heat fluxes were positive during the whole drift with F_H ranging
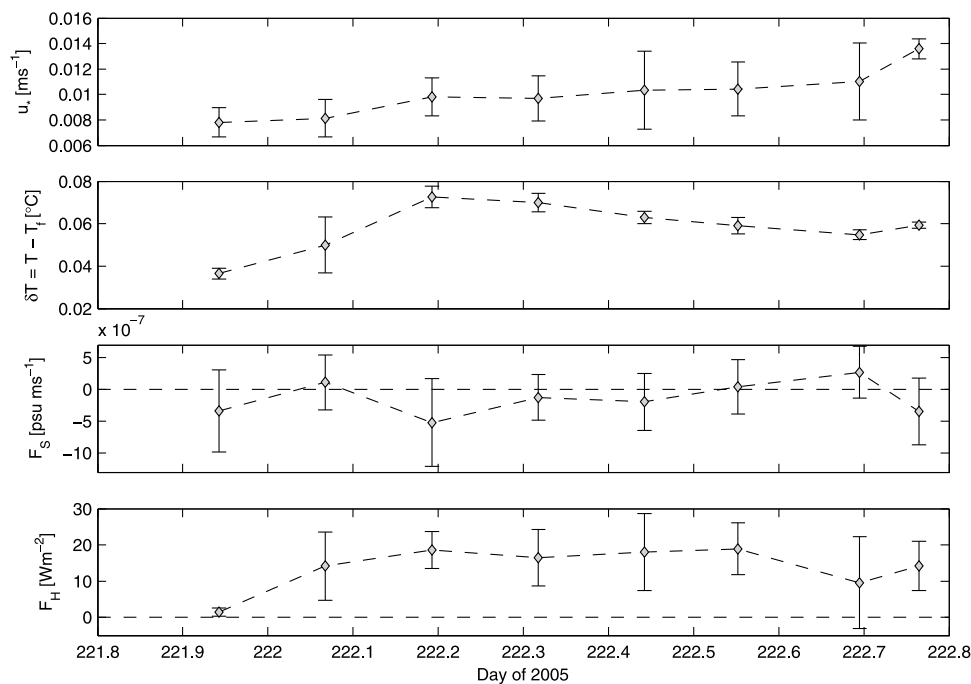
Figure 4. The 3 h averages of friction velocity (u_*), mixed layer temperature elevation above freezing (∂T), salt flux (F_S), and heat flux (F_H) for the P2D1 drift. All values are from the TIC at 2.8 m depth, except F_S, which is from the TIC at 6.8 m. The error bars indicate ±1 standard deviation within the 3 h period.

from 0 W m^{-2} to 27 W m^{-2}, and average heat flux was 13.8 W m^{-2}. During the ANZFLUX Maud Rise drift in 1994, the average heat flux was 23.4 W m^{-2} in almost the same location and at the same time of year [*McPhee et al.*, 1999]. Salt fluxes at 6.8 m were small, fluctuated around zero, and had an average value of 2.1×10^{-8} psu m s^{-1} (Figure 4).

[27] During P2D2, average u_* was 0.56 cm s^{-1} (Figure 5), about half the P2D1 average value. The reduction is due to lower drift and current velocities; however, u_* indicates that the P2D2 ice floe also had smooth under-ice topography. Heat fluxes were always positive, ranging from 1 W m^{-2} to 82 W m^{-2} with an average value of 28.0 W m^{-2}. The mixed layer temperature elevation above freezing (Figure 5) shows that the P2D2 mixed layer contained more heat than P2D1, which is reflected in the higher heat fluxes. P2D2 also displayed a larger temporal variability in mixed layer temperature, salinity, and ice drift velocity, which resulted in larger variability in the interface fluxes. For P2D2, salt fluxes were predominantly negative, with an average value of -3.9×10^{-6} psu m s^{-1}.

[28] For the midlevel mast in the period 227.75–228.63, average values of friction velocity, heat flux, and salt flux were 0.39 cm s^{-1}, 20.7 W m^{-2}, and 4.6×10^{-6} psu m s^{-1}, respectively (Figure 5). The most distinct feature of the measurements at 30.6 m depth was the shift in heat flux around 228.3, where fluxes go from negative (average ~ -9 W m^{-2}) to large positive (average ~ 71 W m^{-2}). Salt fluxes at 30.6 m were of the same magnitude as at 2.8 m but with opposite sign.

4. Discussion

4.1. Dynamics of the Ice Drift

[29] The drift of the ice was clearly controlled by the wind and was modulated by oscillations at the inertial or semidiurnal frequency. Using the complex demodulation technique of *McPhee* [1990], complex position data are fitted to a function containing a mean velocity and oscillating clockwise and counterclockwise components at the inertial and diurnal frequencies. The function is fitted to the data over one diurnal period, and the function coefficients are evaluated every 3 h.

Table 1. Mean Values of Friction Velocity, Heat Flux, Salt Flux, and Eddy Viscosity for Both Drifts[a]

Drift	u_* (cm s^{-1})		F_H (W m^{-2})		F_S (psu m s^{-1})		K_m (m^2 s^{-1})	
	TIC	Model	TIC	Model	TIC	Model	TIC	Model
P2D1	1.00	...	13.8	...	2.1×10^{-8}	...	0.0081	...
P2D2	0.56	0.57	28.0	31.5	-3.9×10^{-6}	-1.3×10^{-6}	0.0044	0.0063

[a]Turbulence instrument cluster (TIC) values are measured at 2.8 m below the ice; model values are from the steady state local turbulence closure (SLTC) model, also at 2.8 m. For P2D2, the model and the TIC measurements cover the same period. Salt fluxes (F_s) are from 6.8 m for P2D1 and 2.8 m for P2D2.
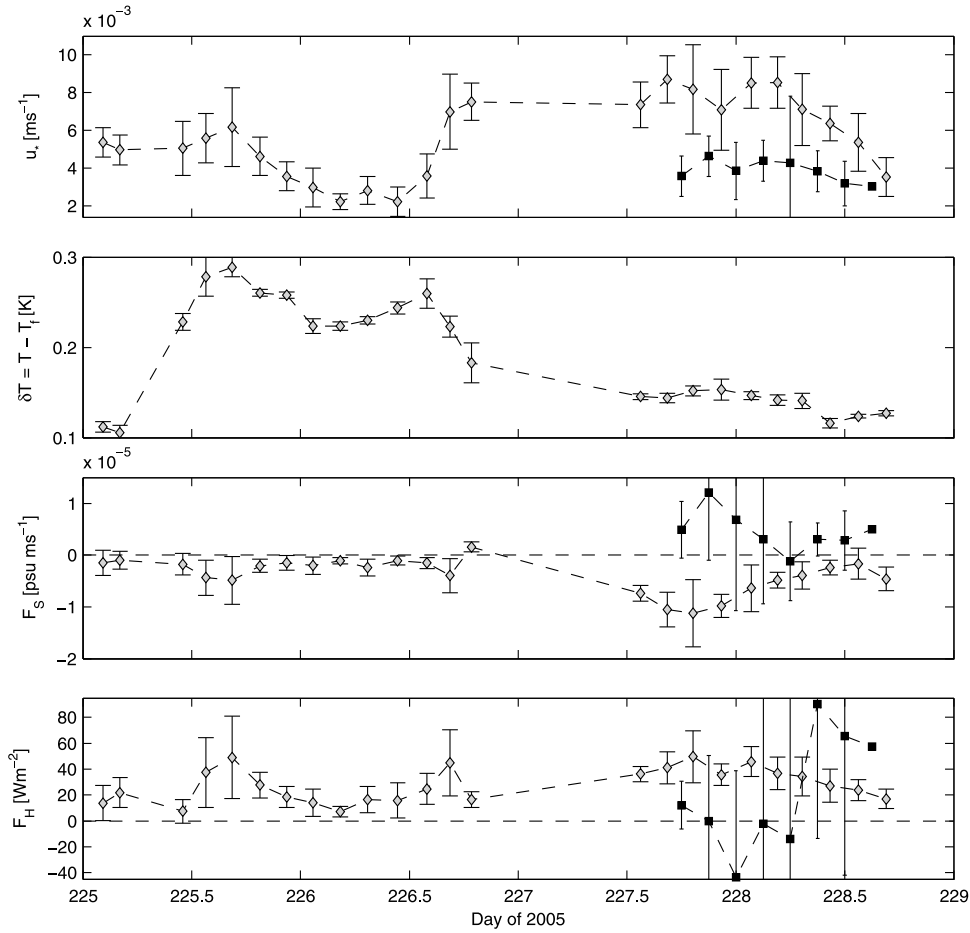
Figure 5. The 3 h averages of friction velocity (u_*), mixed layer temperature elevation above freezing (∂T), salt flux (F_S), and heat flux (F_H) for the P2D2 drift. The gray diamonds are from shallow mast TIC at 2.8 m depth, and the solid squares are from the midlevel mast at 30.6 m. The error bars indicate ±1 standard deviation within the 3 h period.

[30] By separating the ice drift velocity vector into inertial (and diurnal) components and a mean component, we are able to examine the mean ice drift velocity compared with wind velocity. By considering only those periods where wind speeds are larger than 4 m s^{-1} (100% and 92% of time for P2D1 and P2D2, respectively), we find the ratio of mean ice drift velocity to 10 m wind speed to be 3.7% and 2.6% for P2D1 and P2D2, respectively. In general, the drift directions were to the left of the wind, on average 16° for P2D1 and 9° for P2D2. The wind-induced drift is close to previously reported values for wintertime conditions and thin first-year ice in the Weddell Sea. *McPhee et al.* [1996] reported ice drift speeds of 3.1% and 3.8% of the wind speed and ice drift direction about 15° to the left of the wind for the 1994 ANZFLUX study. Similar studies in 1986 by *Martinson and Wamser* [1990] also presented ice drift with velocity magnitudes 3.0% of wind speed (3.2% after adjusting to 10 m wind [*McPhee et al.*, 1996]) and ice drift 23° to the left of the wind.

[31] Mean ice drift and wind velocity are also highly correlated (correlation coefficients 0.82/0.88 for P2D1/P2D2), which confirms that ice was drifting freely with the wind.

4.2. Ice-Ocean Interface Fluxes

[32] For horizontally homogeneous conditions, ocean heat flux and conductive heat flux through the ice are balanced by melting or freezing at the ice-ocean interface:

$$F_H + k_i \frac{\partial T}{\partial z} = \dot{h}\rho_i L, \qquad (4)$$

where k_i is the thermal conductivity of sea ice, $\partial T/\partial z$ is the vertical temperature gradient in the ice, $\dot{h}$ is the ice growth rate, ρ_i is the density of sea ice, and L is the latent heat of fusion for sea ice. Similarly, when considering a small volume at the ice-ocean interface, input of salt water or freshwater from freezing or melting is balanced by the turbulent salt flux toward the interface:

$$F_S = \frac{\rho_i}{\rho} \dot{h}(S_i - S_o), \qquad (5)$$

where S_i and S_o are the ice and ocean surface layer salinities, respectively.

[33] During P2D1, only snow and ice thicknesses were measured (section 2.2). By assuming a linear temperature

gradient through both ice and snow, set by the average ocean and air temperatures, and thermal conductivity of snow and ice to be 0.15 W K^{-1} m^{-1} [*Sturm et al.*, 1997] and 2.1 W K^{-1} m^{-1} [*Trodahl et al.*, 2001], respectively, the ice-snow interface temperature is found, and an average conductive heat flux of 24 W m^{-2} is calculated. This is almost twice the average ocean heat flux and indicates freezing of 0.4 cm ice at the interface to balance equation (4) (using L for sea ice with temperature $-2°$C and salinity of 10 psu). According to equation (5), this results in an average salt flux of -1.5×10^{-6} psu m s^{-1}. Measured F_S differs from this estimate, in both magnitude and sign, which might be due to an underlying salinity gradient as indicated in Figure 2. From a background salinity gradient, a Reynolds flux can be estimated using the eddy diffusivity of salt, $F_S = -K_S(\partial S/\partial z)$. The salinity gradient in the overlapping period of P2D1 (222.6–222.8) is estimated from the average mixed layer salinity and salinity at 2.8 m to be -2.5×10^{-4} psu m^{-1}. When assuming a diffusivity of salt equal to the eddy viscosity calculated from TIC measurements, $K_m = \lambda u_*$, using $K_S = 0.0081$ m^{2}s^{-1} results in $F_S = 2 \times 10^{-6}$ psu m s^{-1}. This is of the same order as the estimated salt flux from freezing at the interface but with opposite sign and shows that the surface stress combined with a background salinity gradient overpowers the surface salinity flux from freezing, and hence, the measured salinity flux is small.

[34] During P2D2, repeated ice thickness measurements indicated that the ice thicknesses remained relatively unchanged. Temperatures were measured at the ice-ocean interface and were combined with average ocean interface temperatures and ice thicknesses to calculate conductive heat fluxes. Averaged over three sections of ice thickness and ice temperature measurements performed during P2D2, the conductive heat flux was found to be 40 W m^{-2}. This is roughly 10 W m^{-2} larger than the average ocean heat flux, which, according to equation (4), is balanced by a net ice growth of 1.2 cm during the 92 h drift. Temperatures at the ice-ocean interface were measured by removing the snow. Since air temperatures were lower than ice temperatures, the ice surface would cool, and actual ice temperatures were higher than measured. This will overestimate the temperature gradient in the ice; hence, the conductive heat flux is an upper estimate. According to equation (5), the estimated freezing equals a salt flux of -1×10^{-6} psu m s^{-1}, which is about three times less than the average measured salt flux. This discrepancy might indicate that processes in addition to freezing/melting at the interface contributed to the salinity variance.

[35] Earlier studies have shown that F_H under drifting sea ice can be related to the product of interface friction velocity (u_{*0}) and the temperature elevation above freezing (δT) via the turbulent transfer coefficient (c_H) [e.g., *McPhee*, 1992]:

$$\langle w'T' \rangle = c_H u_{*0} \delta T. \qquad (6)$$

Further, c_H has shown to be remarkably constant for a large variety of conditions [*McPhee*, 1992; *McPhee et al.*, 1999], and *McPhee et al.* [2008] recommend $c_H = 0.0057$ on the basis of data from several Arctic and Antarctic experiments.

[36] For each drift, c_H was estimated by linear regression through the origin of $\langle w'T' \rangle$ against $u_* \delta T$ for all the 15 min intervals (81 and 252 for P2D1 and P2D2, respectively).

Average c_H for P2D1 was 0.0059 ± 0.0006, indicating the mean and the 95% confidence interval. This is in the same range as previously cited studies. Similarly, for the P2D2 data, the overall c_H was 0.0069 ± 0.0004, slightly higher than estimates from the literature. During P2D2, the redeployment (after day 227.5) initiated a period where heat fluxes were higher than one would predict with a coefficient of 0.0057. The estimates of c_H before and after the redeployment were 0.0059 ± 0.0005 and 0.0083 ± 0.0004, respectively. We explore possible explanations for the enhanced c_H during P2D2 in section 4.5.

## 4.3. Mixing Length, Under-Ice Roughness, and Turbulent Kinetic Energy Balance

[37] Turbulent exchange can often be characterized by a velocity scale and a length scale representing the distance (mixing length, λ) over which the most energetic eddies are effective at transporting momentum. Previous studies have shown a close association between λ and the inverse of the peak at the weighted variance spectrum of vertical velocity [*McPhee and Martinson*, 1994; *McPhee*, 2008a], $\lambda = c_\lambda/k_{max}$, where k_{max} is the wavenumber at the spectral peak and c_λ is a constant, determined empirically to 0.85 [*McPhee*, 1994].

[38] For the TIC data, wavenumber spectra of vertical velocities are calculated for every 15 min interval, and spectral estimates are smoothed and averaged in wavenumber bins. Mixing length is then determined using hourly averaged spectra. Calculations show that mixing lengths at 2.8 m below the ice-ocean interface were relatively constant throughout both P2D1 and P2D2 with average values of 0.86 m and 0.76 m for P2D1 and P2D2, respectively. For P2D2, mixing lengths increased slightly toward the end of the drift. In a neutrally stable boundary layer, the surface layer mixing length is in general limited by the distance from the ice-ocean boundary, $\lambda = \kappa|z|$, where $\kappa = 0.4$ is the von Karman constant and z is the vertical distance from the interface. Farther away from the boundary, the mixing length tends to be limited by the planetary length scale, $\Lambda_* u_*/f$, where u_* is the local friction velocity, f is the local Coriolis parameter, and Λ_* is a similarity constant set to 0.028 [*McPhee et al.*, 1999]. In Figure 6, bin-averaged hourly values of mixing length for both P2D1 and P2D2 are plotted against u_* together with the theoretical geometric and planetary length scales. It seems that λ at 2.8 m was limited by the distance from the interface; however, there also seems to be a decrease in λ for smaller values of u_*, indicating, as also argued by *McPhee* [2008a], that the planetary length scale can be limiting, even at relatively shallow depths. Significant negative salt fluxes were measured toward the end of P2D2 as a possible result of enhanced freezing at the surface or convection. This alters the neutral stratification and can result in larger mixing lengths as was observed in the same period.

[39] The under-ice roughness length, z_0, is related to the ratio of mean velocity and friction velocity by the so-called law of the wall (LOW):

$$\frac{U(z)}{u_*} = \frac{1}{\kappa} \ln \frac{|z|}{z_0}, \qquad (7)$$

where z is the measurement depth. Using hourly mean values of U/u_*, z_0 is estimated to be 1.0×10^{-6} m and 1.3×10^{-5} m
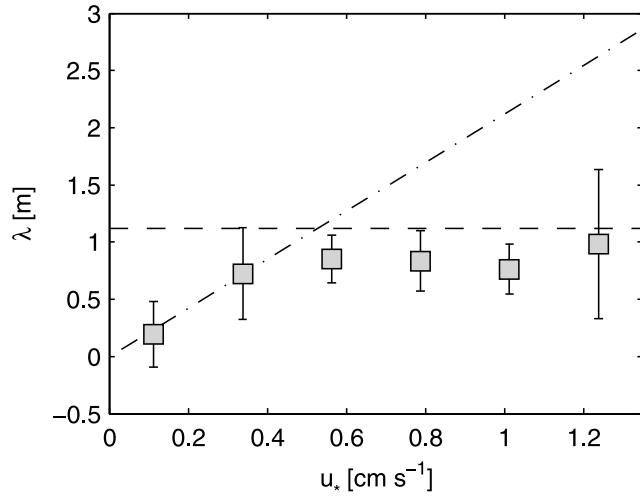
Figure 6. Hourly values of mixing length averaged in friction velocity bins of 1.5×10^{-3} m s^{-1} for TIC measurements at 2.8 m depth for both P2D1 and P2D2. The error bars indicate ± 1 standard deviation. The dashed horizontal line is $\lambda = k|z|$, the limiting scale for mixing length in the surface layer, and dashed-dotted line is the planetary length scale, $\lambda = \Lambda_* u_* / f$.

for P2D1 and P2D2, respectively. These values are very small and confirm the "supersmooth" conditions that were indicated by low u_* values in section 3.3. Further, z_0 calculated from the LOW is actually smaller than it would be for a hydraulically smooth surface, estimated from surface stress and molecular viscosity, $z_0 = (v/u_{*0})e^{-2}$ [*Hinze*, 1959], which gives values of 1.9×10^{-5} m and 2.4×10^{-5} m for P2D1 and P2D2, respectively. This indicates that the LOW might not be the best way to address the measurements at 2.8 m and that effects of the local under-ice topography might affect the surface roughness calculations. Other studies [*Crawford et al.*, 1999; *McPhee*, 1990; *McPhee et al.*, 2008] have shown that the under-ice flow can be well estimated using Hinze's approximation of surface roughness; however, in our case this is not appropriate either. To examine if the calculated surface roughness is representative for the entire floe, the problem is addressed using a steady state 1-D model (section 4.4).

[40] In a steady state turbulent flow, when divergence of turbulent kinetic energy (TKE) and pressure velocity covariance is neglected, shear and buoyancy production of TKE (P_S and P_B, respectively) are balanced by the dissipation rate of TKE (ε), $P_S + P_B = \varepsilon$; P_S can be calculated as $P_S = u_*^3/\lambda$ using λ determined from the weighted spectra of vertical velocity. From the hourly averaged weighted spectra of vertical velocity, the inertial subrange was identified as the wavenumber band where the slope was $-2/3$ (equivalent to the $-5/3$ slope in unweighted spectra). If a distinct subrange existed, ε was calculated according to

$$\varepsilon^{2/3} = \frac{3}{4\alpha_\varepsilon} S_{ww} k^{5/3}. \tag{8}$$

In equation (8), values of wavenumber k and spectral density S_{ww} are from the inertial subrange and $\alpha_\varepsilon = 0.51$ is a

constant [*Edson et al.*, 1991; *McPhee et al.*, 2008]. Further, P_B is calculated as

$$P_B = -\langle w'b'\rangle = -g(\beta_S \langle w'S'\rangle - \beta_T \langle w'T'\rangle) \tag{9}$$

following the sign convention of, e.g., *McPhee and Morison* [2001]. In equation (9), g is the gravity constant and β_S and β_T are the saline contraction coefficient and thermal expansion coefficient, respectively. Moreover, P_S, P_B, and ε are plotted in Figures 7 and 8 for P2D1 and P2D2. For the first drift, the average shear production was 1.5×10^{-6} m^2 s^{-3}, which was nearly balanced by the average dissipation rate of 2.0×10^{-6} m^2 s^{-3}; P_S increased toward the end of the drift, together with increasing values of u_*. Also, for P2D2, average P_S (3.7×10^{-7} m^2 s^{-3}) nearly balanced ε (5.1×10^{-7} m^2 s^{-3}). Because of relatively small salt fluxes during both P2D1 and P2D2, values of P_B were 3 and 2, respectively, orders of magnitude smaller than P_S and ε. This generally justifies neglecting this term as a significant factor in the TKE budget. However, there was a period in the second half of P2D2 where shear production was persistently less than the dissipation rate. In the same period, there was a significant downward salt flux that acted as a source of TKE and in this period P_B accounted for about 25% of the discrepancy between P_S and ε. In general, large negative salt fluxes can be related to enhanced freezing at the surface but have also been observed as a result of convective plumes of brine from warming ice [*Widell et al.*, 2006]. However, since no significant ice freezing was observed, and there were no warming events during P2D2, these are not the likely processes behind the enhanced salt fluxes. It is more likely that this is a result of either convective mixing resulting from differential advection of a horizontal density gradient or cooling/freezing in open water upstream of the measurement site.

4.4. Steady Model Comparison

[41] As discussed in section 4.3, z_0 calculations indicated that the ice underside was "supersmooth," differing from earlier observations of drifting first-year ice in the Weddell Sea. The horizontal footprint of undersurface roughness elements contributing to hydraulic roughness depends on both u_* and the distance from the boundary; hence, measurements near the boundary may not adequately represent z_0 typical of the entire floe [e.g., *McPhee*, 2002]. In this section we utilize a 1-D steady state local turbulence closure model (SLTC model) to characterize "floe-scale" surface roughness and as a tool to supplement measurements in the data analysis.

[42] The model is initiated from the actual vertical profiles of temperature and salinity and is forced with the measured horizontal velocity at a specified depth and the surface stress obtained from the ice drift. In addition, parameters such as under-ice roughness, exchange coefficients at the interface, and ice and snow thickness are specified. From the initial conditions, a first guess of eddy viscosity is made. This is used to calculate turbulent fluxes that will again affect the eddy viscosity, which is then recalculated. This iteration is continued until the difference between modeled and measured velocity at the specified depth is less than a predetermined threshold. The model is described in closer detail by *McPhee* [2008b].
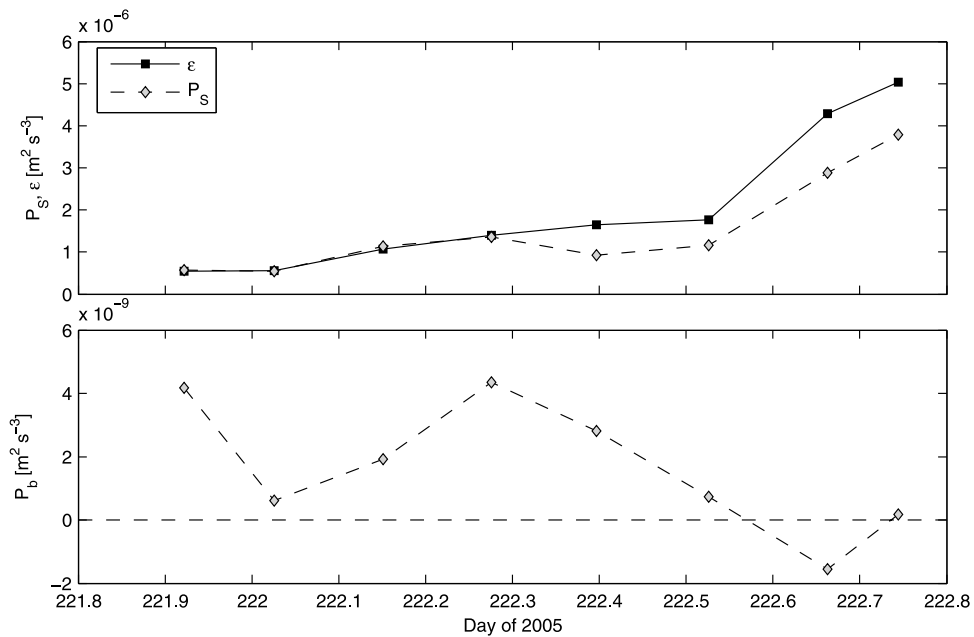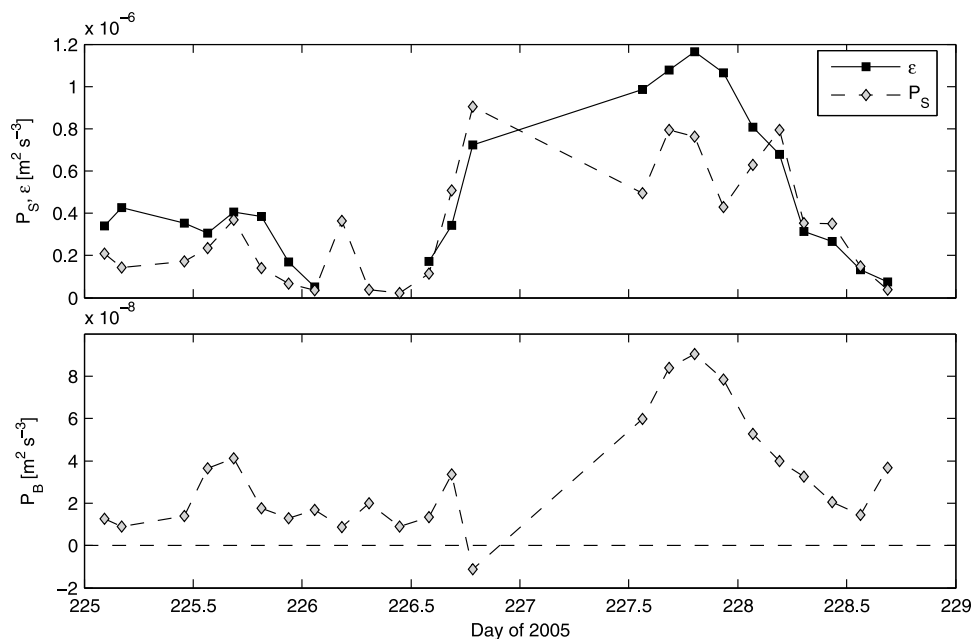
Figure 7. The 3 h averaged values of shear production (P_S), dissipation rate (ε), and buoyancy production (P_B) of TKE for the P2D1 drift. All values are calculated from the TIC at 2.8 m depth, except P_B, which is inferred from the turbulent salt flux at 6.8 m.

[43] For P2D2, the model was set up with 160 levels, spanning 80 m in the vertical. The 3 h averages of TIC, ADP, and CTD measurements were used as initial conditions, and the model was run separately for each interval, providing a time series of steady state variables. The modeled velocity was set to match the measured velocity at 20 m depth, which is assumed to be far enough from the surface to be representative of the floe in general. Under-ice roughness was set to $z_0 = 1.3 \times 10^{-5}$ m; conductive heat flux in the ice was equal to 40 W m^{-2}; and snow and ice thicknesses were set to 0.14 m and 0.40 m.

[44] In Figure 9, average measured velocities from 3 m to 29 m are nondimensionalized by the velocity at 29 m and are plotted together with the equivalent modeled velocity profile for two different values of z_0. Using $z_0 = 1.3 \times 10^{-5}$ m, as inferred from the TIC measurements, clearly underestimates the angular turning of velocity observed in the upper 29 m, and in order to reproduce the observed turning, a

Figure 8. The 3 h averaged values of shear production (P_S), dissipation rate (ε), and buoyancy production (P_B) of TKE for the P2D2 drift. All values are calculated from the TIC at 2.8 m depth.
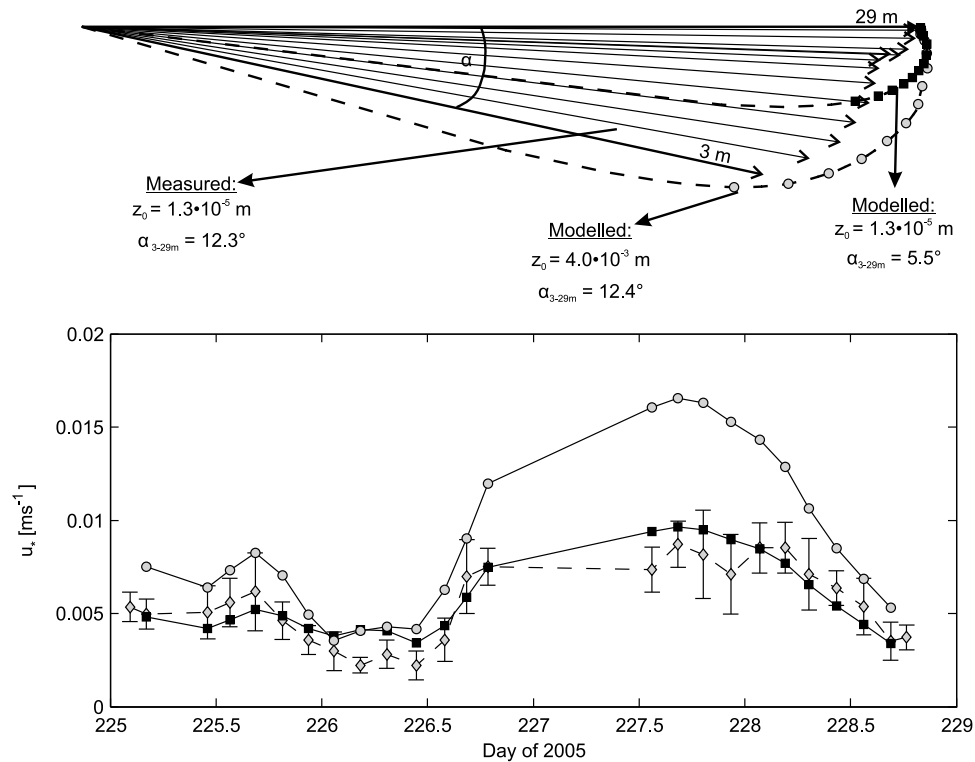
Figure 9. Arrows show relative velocities from 3 m to 29 m nondimensionalized by the velocity at 29 m, averaged over the entire P2D2. The solid squares and gray circles are corresponding velocities from the SLTC model using $z_0 = 1.3 \times 10^{-5}$ m (squares) and $z_0 = 4 \times 10^{-3}$ m (circles), respectively. Angles of turning from 3 m to 29 m are given. The lower part shows measured 3 h averaged friction velocities at 2.8 m depth with the error bars that indicate ±1 standard deviation (diamonds). The solid squares and gray circles are friction velocities from the SLTC model at 2.8 m depth using same values for z_0 as indicated at top.

larger $z_0 = 4 \times 10^{-3}$ m had to be used. When comparing modeled and observed u_* at 2.8 m below the ice (Figure 9, lower part), it is clear that even though the model reproduces the observed angular shear when using $z_0 = 4.0 \times 10^{-3}$ m, it overestimates u_*. However, the modeled u_* using $z_0 = 1.3 \times 10^{-5}$ m fits the observed u_* fairly well. These results indicate that the ice at the measurement site was smoother than the surrounding ice in general and that turbulence measurements made at 2.8 m below the ice might reflect the local ice topography and might therefore not be representative of the entire floe.

[45] Modeled fluxes of heat and salt and the eddy viscosity at 2.8 m depth are plotted and compared with measured values in Figure 10, and average values are summarized in Table 1. In the model, heat fluxes are estimated from surface stress and mixed layer temperature (equation (6)), and they generally show a good agreement with the measured heat fluxes. Modeled salt fluxes are calculated from the heat balance at the ice-ocean interface, using excess/deficit heat to melt/freeze ice and hence input salt/meltwater to the surface layer. Modeled eddy viscosity at 2.8 m shows reasonable agreement with $K_m = u_* \lambda$ calculated from the TIC measurements. The average modeled salt flux is roughly comparable to the measured (-1.3×10^{-6} psu m s^{-1} versus -3.9×10^{-6} psu m s^{-1}); however, the modeled salt flux displays variability different from the observed salt flux. The comparison of salt fluxes indicates

that surface fluxes not only are determined by 1-D thermo-dynamic processes at the ice-ocean interface but are affected by horizontal variability in both water mass and ice properties.

4.5. Horizontal Variability

[46] Horizontal variability in water masses and/or ice conditions can in general violate the general assumption of horizontal homogeneity when considering turbulence dynamics. During P2D2, there were some events that suggested such an influence from additional sources of turbulence: (1) There was a period with large negative salt fluxes (227.5–228.5) when heat balance at the interface indicates that salt fluxes should be positive. (2) In the same period, there was a significant gap between shear production and dissipation rate of TKE. (3) In the same period, an overall mismatch between the observed velocity turning in under-boundary layer and the velocity turning given by the SLTC model (which assumes horizontal homogeneity) were seen.

[47] A horizontal variability in salinity (or density) over a relatively short distance might act as an additional source or sink of turbulent energy. This has been indicated by several studies [e.g., *Crawford et al.*, 1999; *Rippeth et al.*, 2001; *Stacey and Ralston*, 2005], where a horizontal density gradient, often in combination with a strong tidal flow, altered the stratification in the boundary layer and led to
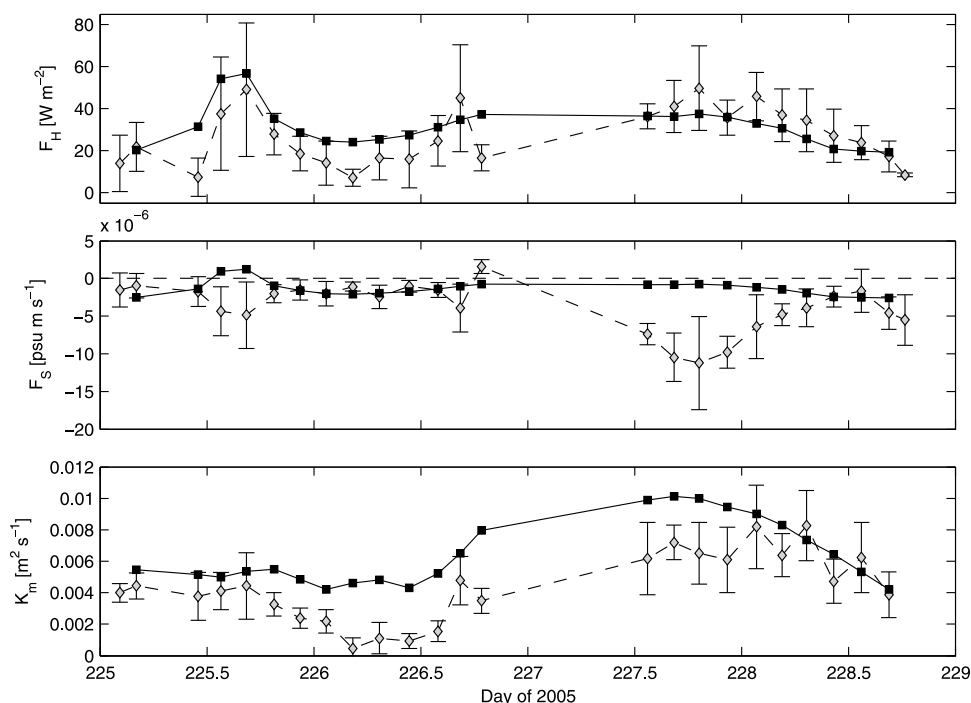
Figure 10. Comparison of measured and modeled heat fluxes (F_H), salt fluxes (F_S), and eddy viscosity (K_m) at 2.8 m depth for the P2D2 drift. The gray diamonds are the 3 h averaged TIC values, and the error bars indicate ±1 standard deviation. The solid squares are modeled values using $z_0 = 1.3 \times 10^{-5}$ m for the same 3 h periods.

enhanced or reduced turbulence. In some cases, this contributed with a production of TKE that was up to 50% of the shear production, i.e., an important term in the overall TKE budget [*Stacey and Ralston*, 2005]. In the under-ice boundary layer a nonuniform velocity profile will advect a horizontal density gradient faster at depth than close to the ice. In case of a negative horizontal density gradient, this might lead to situations with a temporarily unstable stratification, which again will overturn and lead to enhanced TKE and turbulent fluxes in the boundary layer. During 227.5–228.5, the ice drifted over gradually fresher water, implying a negative horizontal density gradient in the mixed layer, which could lead to temporal instabilities and convection. This could be a possible explanation for enhanced heat fluxes, negative salt fluxes, and an additional source of TKE to balance the observed excess of dissipation rate of TKE in this period.

[48] The presence of a horizontal density gradient (i.e., a horizontal pressure gradient) might also influence the angular shear of velocity in the under-ice boundary layer, as the pressure gradient will be balanced by vertical gradient of horizontal velocity. This is described by the so-called thermal wind equation,

$$\frac{\partial v}{\partial z} = -\frac{g}{\rho_0 f}\frac{\partial \rho}{\partial x}$$

[e.g., *Pond and Pickard*, 1983], where a density gradient in the drift direction is compensated by a cross-drift vertical velocity shear. As an example, the cross-drift velocity shear is calculated for the period 227.5–228.5 when there was a

negative horizontal density gradient as the ice drifted from Taylor Cap water and into Halo water. By integrating $\partial v/\partial z$ over the range of the ADP measurements (3–29 m), the cross-drift velocity component due to the horizontal density gradient is found. This component is then rotated into the east–north reference frame and is subtracted from the measured velocities in order to find the velocities without influence of horizontal gradients. The observed angular turning from 3 m to 29 m in this given period was 9.7°; after correcting for "thermal wind," the angular turning was 6.7°, close to the modeled angular turning of 7.1°.

[49] Toward the end of P2D2, there was an increasing amount of leads surrounding the floe. During winter, leads are areas of rapid cooling and freezing and hence areas of convection acting as additional sources of TKE. An upstream source of TKE can show up in the upper part of the boundary layer as a distinct excess of dissipation rate of TKE compared with shear production [*McPhee*, 2004]. This way, a nearby convecting lead can produce TKE that is distributed in the boundary layer and is transported as vertical flux of TKE from below and toward the surface layer at the measurement site, which is suggested from the TKE discrepancy for 227.5–228.5.

5. Summary

[50] This study presents and discusses key aspects of the boundary layer under the drifting sea ice in the eastern Weddell Sea and is important for the MaudNESS experiment, as well as for the general understanding of the wintertime Weddell Sea air-sea-ice interaction. During the two drifts, P2D1 and P2D2 on top and on the flank of the Maud Rise,

respectively, the following characteristics of the ice and the under ice boundary layer were found:

[51]   1. Ice was drifting with an average speed of 3.7% and 2.6% of the wind speed, respectively, and drift directions were on average 16° and 9° to the left of the wind. In general, the mixed layer oscillated in phase with the ice at the inertial or semidiurnal tidal frequency. However, for P2D2, baroclinic flow components were visible in the lower mixed layer because of horizontal density gradients. TIC measurements at 2.8 m indicated roughness lengths of 1.0×10^{-6} m and 1.3×10^{-5} m, less than would be expected if the surface were hydraulically smooth. Comparison with steady state turbulence model suggests that these small roughness lengths are not representative of the entire ice floe but rather of the local ice topography at the measurement site.

[52]   2. Heat fluxes were 13.8 W m^{-2} and 28.0 W m^{-2} for P2D1 and P2D2, both slightly smaller than the estimated conductive heat flux in the ice, which indicates that freezing did take place at the interface to balance heat fluxes. No significant changes in ice thickness were observed; however, average salt fluxes of 2.1×10^{-8} psu ms^{-1} and -3.9×10^{-6} psu ms^{-1} were measured for P2D1 and P2D2, respectively. Linear regression of kinematic heat flux against the product of friction velocity and mixed layer temperature elevation above freezing resulted in an overall average heat transfer coefficient of 0.0067 ± 0.0008, slightly higher than estimates from other studies.

[53]   3. Mixing length seemed to be limited by the vertical distance from the ice-ocean interface for both drifts. However, for low-friction velocities, the planetary length scale seems to be an important scale for turbulence in the surface boundary layer.

[54]   4. Shear production due to ice drift was the main source of TKE. However, in some periods during P2D2, enhanced turbulent fluxes, a discrepancy between shear production and dissipation rate of TKE, and an enhanced angular turning of velocity with depth implied possible influence of horizontal gradients in water mass properties and an increasing fraction of open leads in the area.

[55]   The results presented here give a picture of the delicate balance of wind, ice, dynamics, and thermodynamics in the Weddell Sea air-sea-ice interaction. The relatively weak pycnocline makes heat transfer from the warm deeper layer to the mixed layer effective and variable; mixing in the surface layer is highly set by the wind-forced ice drift, also largely varying in speed and direction. This interplay includes processes that on average can be estimated using relatively simple models and parameterizations. However, the current study also shows that the Weddell Sea is an area with large variability and a suite of additional processes that contribute to drive the air-sea-ice interaction on shorter time scales.

References

Akitomo, K. (1999a), Open-ocean deep convection due to thermobaricity: 1. Scaling argument, *J. Geophys. Res.*, *104*(C3), 5225–5234, doi:10.1029/1998JC900058.

Akitomo, K. (1999b), Open-ocean deep convection due to thermobaricity: 2. Numerical experiments, *J. Geophys. Res.*, *104*(C3), 5235–5249, doi:10.1029/1998JC900062.

Carsey, F. D. (1980), Microwave observation of the Weddell polynya, *Mon. Weather Rev.*, *108*(12), 2032–2044, doi:10.1175/1520-0493(1980)108<2032:MOOTWP>2.0.CO;2.

Crawford, G., L. Padman, and M. McPhee (1999), Turbulent mixing in Barrow Strait, *Cont. Shelf Res.*, *19*(2), 205–245, doi:10.1016/S0278-4343(98)00086-7.

De Steur, L., D. M. Holland, R. D. Muench, and M. G. McPhee (2007), The warm-water "Halo" around Maud Rise: Properties, dynamics and impact, *Deep Sea Res., Part I*, *54*(6), 871–896, doi:10.1016/j.dsr.2007.03.009.

Edson, J. B., C. W. Fairall, P. G. Mestayer, and S. E. Larsen (1991), A study of the inertial-dissipation method for computing air-sea fluxes, *J. Geophys. Res.*, *96*(C6), 10,689–10,711, doi:10.1029/91JC00886.

Gordon, A. L. (1978), Deep Antarctic convection west of Maud Rise, *J. Phys. Oceanogr.*, *8*(4), 600–612, doi:10.1175/1520-0485(1978)008<0600:DACWOM>2.0.CO;2.

Gordon, A. L. (1991), Two stable modes of Southern Ocean winter stratification, in *Deep Convection and Deep Water Formation in the Oceans*, edited by C. Chu and J. C. Gascard, pp. 17–35, Elsevier, Amsterdam.

Gordon, A. L., and B. A. Huber (1990), Southern-ocean winter mixed layer, *J. Geophys. Res.*, *95*(C7), 11,655–11,672, doi:10.1029/JC095iC07p11655.

Hinze, J. O. (1959), *Turbulence*, 586 pp., McGraw-Hill, New York.

Martinson, D. G., and C. Wamser (1990), Ice drift and momentum exchange in winter Antarctic pack ice, *J. Geophys. Res.*, *95*(C2), 1741–1755, doi:10.1029/JC095iC02p01741.

McPhee, M. G. (1990), Small-scale processes, in *Polar Oceanography*, edited by W. Smith, pp. 287–334, Academic, San Diego, Calif.

McPhee, M. G. (1992), Turbulent heat-flux in the upper ocean under sea ice, *J. Geophys. Res.*, *97*(C4), 5365–5379, doi:10.1029/92JC00239.

McPhee, M. G. (1994), On the turbulent mixing length in the oceanic boundary-layer, *J. Phys. Oceanogr.*, *24*(9), 2014–2031, doi:10.1175/1520-0485(1994)024<2014:OTTMLI>2.0.CO;2.

McPhee, M. G. (2000), Marginal thermobaric stability in the ice-covered upper ocean over Maud Rise, *J. Phys. Oceanogr.*, *30*(11), 2710–2722, doi:10.1175/1520-0485(2000)030<2710:MTSITI>2.0.CO;2.

McPhee, M. G. (2002), Turbulent stress at the ice/ocean interface and bottom surface hydraulic roughness during the SHEBA drift, *J. Geophys. Res.*, *107*(C10), 8037, doi:10.1029/2000JC000633.

McPhee, M. G. (2004), A spectral technique for estimating turbulent stress, scalar flux magnitude, and eddy viscosity in the ocean boundary layer under pack ice, *J. Phys. Oceanogr.*, *34*(10), 2180–2188, doi:10.1175/1520-0485(2004)034<2180:ASTFET>2.0.CO;2.

McPhee, M. G. (2008a), Physics of early summer ice/ocean exchanges in the western Weddell Sea during ISPOL, *Deep Sea Res., Part II*, *55*(8–9), 1075–1097, doi:10.1016/j.dsr2.2007.12.022.

McPhee, M. G. (2008b), *Air-Ice-Ocean Interaction: Turbulent Boundary Layer Exchange Processes*, 215 pp., Springer, New York.

McPhee, M. G., and D. G. Martinson (1994), Turbulent mixing under drifting pack ice in the Weddell Sea, *Science*, *263*(5144), 218–221, doi:10.1126/science.263.5144.218.

McPhee, M. G., and J. H. Morison (2001), Under-ice boundary layer, in *Encyclopedia of Ocean Sciences*, edited by M. Steele et al., pp. 3071–3078, Academic, San Diego, Calif.

McPhee, M. G., S. F. Ackley, P. G. Huber, D. G. Martinson, J. H. Morison, R. D. Muench, L. Padman, and T. P. Stanton (1996), The Antarctic Zone Flux Experiment, *Bull. Am. Meteorol. Soc.*, *77*(6), 1221–1232, doi:10.1175/1520-0477(1996)077<1221:TAZFE>2.0.CO;2.

McPhee, M. G., C. Kottmeier, and J. H. Morison (1999), Ocean heat flux in the central Weddell Sea during winter, *J. Phys. Oceanogr.*, *29*(6), 1166–1179, doi:10.1175/1520-0485(1999)029<1166:OHFITC>2.0.CO;2.

McPhee, M. G., J. H. Morison, and F. Nilsen (2008), Revisiting heat and salt exchange at the ice-ocean interface: Ocean flux and modeling considerations, *J. Geophys. Res.*, *113*, C06014, doi:10.1029/2007JC004383.

Muench, R. D., J. H. Morison, L. Padman, D. Martinson, P. Schlosser, B. Huber, and R. Hohmann (2001), Maud Rise revisited, *J. Geophys. Res.*, *106*(C2), 2423–2440, doi:10.1029/2000JC000531.

Pond, S., and G. L. Pickard (1983), *Introductory Dynamical Oceanography*, 2nd ed., Butterworth-Heinemann, Oxford. U. K.

Rippeth, T. P., N. R. Fisher, and J. H. Simpson (2001), The cycle of turbulent dissipation in the presence of tidal straining, *J. Phys. Oceanogr.*, *31*(8), 2458–2471, doi:10.1175/1520-0485(2001)031<2458:TCOTDI>2.0.CO;2.

Robertson, R., L. Padman, and G. Egbert (1998), Tides in the Weddell Sea, in *Ocean, Ice, and Atmosphere: Interactions at the Antarctic Continental*

Margin, *Antarct. Res. Ser.*, vol. 75, edited by S. S. Jacobs and R. F. Weiss, pp. 341–369, AGU, Washington, D. C.

Smith, S. D. (1988), Coefficients for sea-surface wind stress, heat-flux, and wind profiles as a function of wind-speed and temperature, *J. Geophys. Res.*, *93*(C12), 15,467–15,472, doi:10.1029/JC093iC12p15467.

Stacey, M. T., and D. K. Ralston (2005), The scaling and structure of the estuarine bottom boundary layer, *J. Phys. Oceanogr.*, *35*(1), 55–71, doi:10.1175/JPO-2672.1.

Sturm, M., J. Holmgren, M. Konig, and K. Morris (1997), The thermal conductivity of seasonal snow, *J. Glaciol.*, *43*(143), 26–41.

Trodahl, H. J., S. O. F. Wilkinson, M. J. McGuinnes, and T. G. Haskell (2001), Thermal conductivity of sea ice: Dependence on temperature and depth, *Geophys. Res. Lett.*, *28*, 1279–1282, doi:10.1029/2000GL012088.

Widell, K., I. Fer, and P. M. Haugan (2006), Salt release from warming sea ice, *Geophys. Res. Lett.*, *33*, L12501, doi:10.1029/2006GL026262.

Zwally, H. J., and P. Gloersen (1977), Passive microwave images of the polar regions and research applications, *Polar Rec.*, *18*, 431–450, doi:10.1017/S0032247400000930.

————————————

M. G. McPhee, McPhee Research Company, 450 Clover Springs Rd., Naches, WA 98937, USA.

J. H. Morison, Polar Science Center, Applied Physics Laboratory, University of Washington, 1013 NE 40th St., Box 355640, Seattle, WA 98105-6698, USA.

W. J. Shaw and T. P. Stanton, Naval Postgraduate School Public Affairs Office, Code 004, 1 University Cir., Monterey, CA 93943, USA.

A. Sirevaag, Geophysical Institute, University of Bergen, Allégt. 70, N-5007 Bergen, Norway. (anders.sirevaag@bjerknes.uib.no)